ACS APPLIED POLYMER MATERIALS

pubs.acs.org/acsapm Article

Liquids that Freeze when Mixed: Homogeneous Cocrystallization Kinetics of Polyoxacyclobutane−Water Hydrate

Emily F. Barker,[§] Sudesna Banerjee,[§] Tara Y. Meyer,* and Sachin Velankar*

Cite This: ACS Appl. Polym. Mater. 2022, 4, 703−713 Read Online

ACCESS | Metrics & More | Article Recommendations | Supporting Information

ABSTRACT: We report on the kinetics of crystallization of polyoxacyclobutane (POCB) and water to form a cocrystal hydrate, the first paper to explore the kinetics of crystallization of a polymer with a small molecule. POCB has unusual cocrystallization behavior when mixed with water, which could be exploited for a variety of applications including improving the nonvolatile memory storage capabilities of carbon nanotube devices, water purification, and biomedical applications such as drug delivery. The rates of hydrate crystallization of a series of mixtures containing up to 24 wt % water were measured using both a bulk, volumetric and a localized, spherulite growth approach. At these compositions, all mixtures were single-phase homogeneous liquids prior to hydrate crystallization, and all mixtures were POCB-rich as compared to the cocrystal stoichiometry. The time dependence of crystallization kinetics is well described by the Avrami equation. Reducing temperature, i.e., increasing undercooling, increases the Avrami exponents and increases spherulite growth velocities consistent with the Hoffmann−Lauritzen model. Reducing water content reduces spherulite growth velocities. The velocities also reduce with time during spherulite growth reminiscent of impurity effects in crystallization. Talc was found to accelerate nucleation. Broadly, the cocrystallization process starting from the homogeneous mixtures of the components resembles homopolymer crystallization, but with the complexity that when the mixture composition deviates from the cocrystal stoichiometry, the excess species cannot crystallize fully.

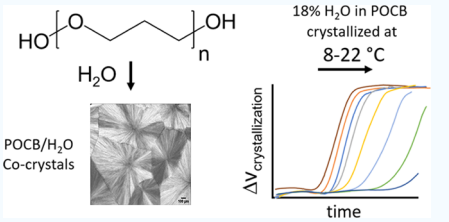

KEYWORDS: *hydrate, clathrate, liquid−liquid equilibrium, crystallization kinetics, spherulite, cocrystal, polymer*

1. INTRODUCTION

Previously,[1] we reported on the phase behavior of mixtures of 650 Da polyoxacyclobutane (POCB) and water. POCB, also known as polytrimethylene oxide (or glycol), polyoxetane, or poly(1,3-propanediol) has the rare ability to cocrystallize with water to form a crystalline hydrate. POCB crystallizes in four distinct forms[2−5] with different chain conformations and unit cells. Three of these are POCB homopolymer crystals. The fourth, called form I, is unusual in that it is a crystalline hydrate with a water/mer ratio of 1:1. Other polymers that can cocrystallize with small-molecule compounds are known,[6−18] but cocrystallization with water is found only in POCB,[2] linear polyethyleneimine,[19] and possibly poly(1,3-dioxolane).[16−18] Exclusive to POCB is its ability to cocrystallize with water near body temperature (37 °C), making POCB of potential interest for medical applications. POCB also exhibits several other unusual and fascinating properties including that pure POCB has an unusually low melting temperature compared to other polyxoyalkylenes, that the melting temperature of the hydrate exceeds that of both of the individual components, and that POCB separates from water upon the melting of the hydrate.[1] These properties could lead to a variety of potential applications, such as improving the nonvolatile memory storage capabilities of carbon nanotube devices,[20] drug delivery or other biomedical applications,[21,22] water purification,[23] materials with high proton and ion conductivity for membrane applications,[24,25] and stimuli-responsive materials.[26] To lay the foundation for such applications, this article moves beyond phase behavior and examines the kinetics of hydrate cocrystallization by dilatometry and by microscopic observations of spherulite growth. The central issues explored here are the dependence of cocrystallization kinetics on mixture composition and temperature.

While the structural and thermodynamic aspects of polymer−small-molecule cocrystallization are well studied,[6,7] there is little information about the kinetics of such cocrystallization.[12,27] As compared to the vast knowledge of crystallization kinetics of homopolymers, polymer blends, or polymer solutions,[28−30] even basic questions about cocrystallization have not been tackled. For example, there is little knowledge of how cocrystallization kinetics depend on temperature, how cocrystallization proceeds with time, or how cocrystallization depends on mixture composition. In polymer crystallization from mixtures, it is well recognized that diffusion limitations of one or both species may affect

Received: November 16, 2021
Accepted: November 24, 2021
Published: December 7, 2021

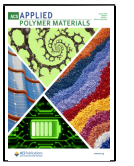

crystallization kinetics.[29,31−34] Because cocrystallization must occur from a mixture of two species, similar diffusion limitations may also be a necessary complexity of cocrystallization. We address some of these questions in this paper. We focus on the kinetics of cooling-induced batch crystallization of POCB/water mixtures with relatively low water content (m_w < 24 wt %), where m_w is the mass percentage of water in the mixture. Low water contents are chosen for this research because, as will be discussed, it is then possible to maintain a single-phase liquid before and during the entire hydrate crystallization process.

Previously, we studied the phase behavior of POCB−water mixtures at a POCB number average molecular weight of 650 Da. Examining the corresponding phase diagram (Figure 1) in

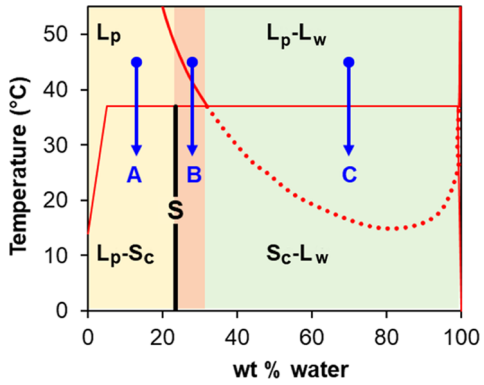

Figure 1. Phase diagram for 650 Da POCB and water. The vertical black line labeled S indicates the composition of the cocrystal hydrate. The solid red line indicates liquid−liquid coexistence between L and L_w phases. The dotted red line indicates a metastable portion of the liquid−liquid coexistence curve. Blue arrows illustrate cooling samples in three different composition regions. (A) Cooling from a homogeneous solution of water and polymer to form POCB/water cocrystals; (B) cooling from a phase-separated mixture through a homogeneous solution to a mixture of cocrystals in equilibrium with a solution of POCB in water; and (C) cooling from a phase-separated mixture directly to a mixture of cocrystals in equilibrium with a solution of POCB in water. The left boundary of the L_p−S_c region is drawn approximately; the full-phase diagram is shown in Banerjee et al.[1]

detail, POCB hydrate has an isostochiometric crystal (1:1 molar ratio of repeat unit to water), corresponding to a composition of m_w = 23.6 wt % water.[2] For the 650 Da polymer, the melting temperature of the hydrate is T_m = 37 °C, which is higher than both the melting temperature of pure water and of pure POCB. Below 37 °C, the solid crystal (S_c) coexists with either the liquid polymer-rich phase (L_p) in the region marked L_p−S_c or the liquid water-rich phase (L_w) in the region marked S_c−L_w. Above 37 °C, the mixture shows either a single homogeneous liquid (L_p) or a coexistence of polymer-rich and water-rich phases (L_p−L_w). Due to the complex phase behavior, the mixture composition has important implications for batch crystallization induced by cooling. Three key composition regions can be distinguished. In region A, with m_w < 23.6 wt %, a single homogeneous L_p phase exists above the melting temperature of the POCB hydrate. Cooling below T_m produces hydrate, while the coexisting L_p phase concomitantly becomes enriched in the polymer as the crystallization proceeds. In region B, where the water content slightly exceeds m_w = 23.6 wt %, it is possible, depending on the initial temperature, to start crystallizing from the homogeneous L_p phase. However, as crystallization proceeds, the L_w phase becomes further enriched in water, and phase separation of the liquid phase may occur. In region C, corresponding to high m_w values, the phase-separated L_p−L_w region appears above $T = T_m$. As the hydrate crystallizes upon cooling below T_m, both phases change in composition until the final S_c−L_w equilibrium is reached. Regions B and C both present significant experimental challenges as phase separation requires the sample to be well mixed to avoid density-based separation of liquid phases. For this reason, this first study focuses on region A only.

Even homopolymer crystallization is a complex phenomenon. A variety of factors contribute to the rate of crystallization, crystal size and shape, thermodynamic stability, and the degree of crystallinity. Two prevalent theoretical frameworks that are widely applied to the crystallization of polymers are the Johnson−Mehl−Avrami−Kolmogorov (JMAK)[28] model, which models the bulk rate of crystallization, and the Hoffman−Lauritzen (HL)[35] model for lamellar growth. It should be noted that these models each have known limitations. The JMAK model does not take into account all of the mechanics of nucleation and growth of lamellar crystals,[36,37] and the HL theory does not capture all molecular aspects of polymer crystallization.[35,38−42] Despite these limitations, these models have been shown to provide significant insight into the crystallization of polymers. One of our aims is to understand whether the cocrystallization of POCB and water can be described using these established theories.

JMAK theory[28] arises from a Poisson relation, as derived by Evans,[43] to model the expanding circles of waves from raindrops landing in a pool of water. According to this theory, crystallization kinetics are characterized by an exponent (n) that describes the dimensionality of growth. The fraction of material crystallized, χ_c, changes as

$$\chi_c = 1 - \exp(-(kt^n)) \quad (1)$$

While the original theory required integer values for n, diffusion-controlled growth can give rise to half-integer values. As well summarized by Lorenzo et al.,[44] deviations from eq 1 can arise for several reasons, e.g., a change in the rate of primary nucleation during the crystallization process or an induction time for crystallization. Avrami exponents often decrease as time increases. It is also possible for a combination of diffusion-controlled growth and time-varying primary nucleation to yield the same exponents with differing mechanisms.[45,46]

The Hoffman−Lauritzen model examines the nucleation and growth of lamellar chain-folded crystals from amorphous chains. As per this theory, the lamellar growth velocity increases approximately exponentially with the reciprocal of the undercooling. This theory has provided insights into changes in the regimes of crystal growth as the undercooling increases, which are reflected in changes in the slope of the plots of spherulite growth velocity vs undercooling.[35]

Although the literature on the kinetics of cocrystallization of polymers with small molecules is sparse, there are some studies on these systems and other related ones that we consider relevant precedents to our current work. In particular, there are several investigations that highlight potential applications for these systems, including the melting-induced delivery of encapsulated drugs[47−50] and the sequestration of impurities

https://doi.org/10.1021/acsapm.1c01626
ACS Appl. Polym. Mater. 2022, 4, 703−713

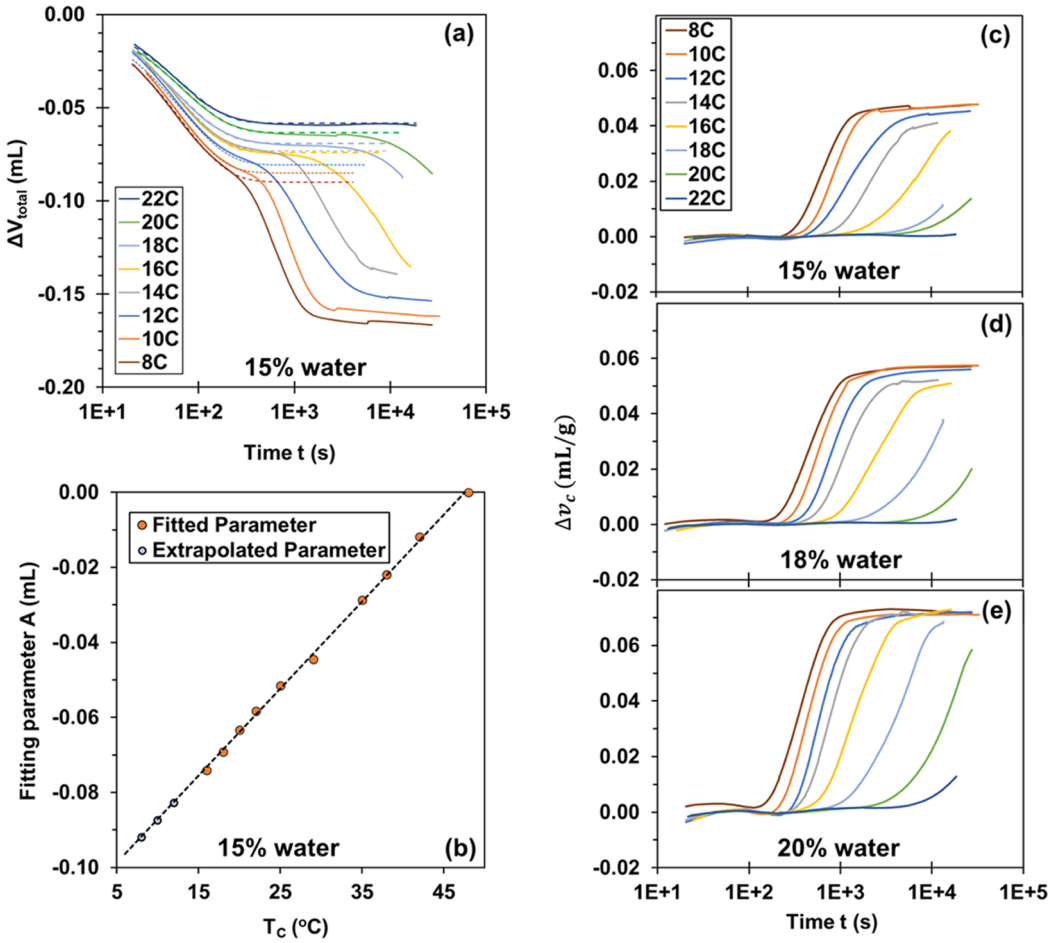

Figure 2. Dilatometry results. (a) Sample with m_w = 15%. Solid lines are experimental measurements of $\Delta V_{total}(t)$. Dashed and dotted lines are volume change due to thermal contraction, ΔV_{tc}, see text. (b) Magnitude of thermal contraction (parameter A in eq 4) corresponding to the data in plot (a). Filled orange circles are obtained from fitting measured data; open black circles are extrapolated from the linear fit (dashed line). (c–e) Specific volume change due to crystallization for mixtures with m_w = 15%, m_w = 18%, and m_w = 20%, respectively.

in water.[51−53] In related, but not fully analogous systems, studies on polymer clathrates and inclusion compounds[6,7,11,54,55] and on the kinetics of vapor sorption of already crystallized polymers[56] are also relevant. Studies on polymer/polymer cocrystallization are also important, many of which include detailed kinetic analyses. These investigations focus on the mixtures of the same polymer but with different molecular weights,[57,58] mixtures of stereoisomers,[27,59] or structurally similar polymers.[60]

This paper is organized as follows. Section 2 describes the materials and methods. In Section 3, we first describe the results of bulk cocrystallization kinetics focusing on how the cocrystallization rate depends on temperature and composition. Next, we describe microscopy experiments and how the spherulitic growth velocity depends on temperature and composition. Section 4 offers a brief discussion of the results and a summary of the paper.

2. EXPERIMENTAL SECTION

2.1. Materials. Polyoxacyclobutane with hydroxyl end groups was obtained from DuPont under the trade name of Cerenol and used without purification. The molecular weight of 650 Da was reported by the manufacturer. Our own gel permeation chromatography, using tetrahydrofuran (THF) as a solvent and polystyrene standards, gave a molecular weight of 567 Da and a dispersity of 1.8.

The glassware used to measure specific volume change was fabricated by the glass shop at the University of Pittsburgh.

The hydrophilic fumed silica was obtained from Wacker Chemical Corporation (HDK N20) and the talc (~200 mesh) was obtained from ACROS Organic.

2.2. Methods. *2.2.1. Volumetric Analysis of Cocrystallization Rates. 2.2.1.1. Apparatus.* Custom-made volume dilatometers (Figure S1) were used for all measurements. The dilatometers consisted of a round-bottom flask with an approximate volume of 4 mL attached via ground glass joint to glass tubes with an approximate length of 12 cm, an inner diameter of 1.11 mm, and an outer diameter of 7.28 mm.

2.2.1.2. Sample Preparation. Mixture compositions are designated by m_w: the mass percentage of water in the mixture. POCB and deionized water were combined to form mixtures ranging from m_w = 8−23.6 wt % water. Prior to loading samples into dilatometers, the mixtures were heated above the melting temperature of the hydrate to achieve a homogenous liquid. An aliquot (1−2 mL) of this mixture was transferred to the dilatometer. The amount of material added was quantified by weight. The dilatometer was assembled and mineral oil (~2 mL) was added to the flask and glass tubing such that the oil meniscus at room temperature sat a few centimeters below the top of the tubing.

2.2.1.3. Volume Change Measurements. Using a custom sample holder (Figure S1), up to five samples were monitored simultaneously. Samples were first equilibrated for at least 15 min at 48 °C to ensure that all crystals were melted. To record volume changes due to crystallization, the samples were rapidly transferred from a hot bath to

https://doi.org/10.1021/acsapm.1c01626
ACS Appl. Polym. Mater. 2022, 4, 703−713

a cold bath maintained at a chosen crystallization temperature, T_c, in the range of 8−22 °C under quiescent conditions. The experiment was photographed at 3.5 s intervals, and the images were analyzed using motion tracking software to determine the position of the meniscus in the glass tubing as a function of time. The volume changes were calculated and normalized for sample weight. At the end of the experiment, the temperature was again increased to 48 °C to provide an accurate meniscus height corresponding to the fully molten sample.

2.2.1.4. Spherulite Growth Rate Measurements. Each sample was first melted above 37 °C and held at that temperature until the sample was a homogeneous liquid with no crystallites present. A drop of the melted liquid was placed between two glass coverslips, with the thickness regulated by 50 μm thick adhesive tape as a spacer. The sample was immediately moved to a temperature-controlled stage under a polarization microscope (Leitz Orthoplan, with a 10x objective), and images were saved at 3.5 s intervals. Due to the relatively low nucleation density, it was necessary to search across the sample to find a growing spherulite, and hence the earliest stages of spherulite growth were difficult to capture. At most sample compositions and temperatures, the spherulites were not precisely circular. To avoid difficulties in tracking the motion of a noncircular perimeter, the growth velocity G was calculated from the evolution of area A during spherulite growth using the equations

$$R = \sqrt{\frac{A}{\pi}} \quad \text{and} \quad G = \frac{dR}{dt} = \frac{1}{\sqrt{4\pi A}}\frac{dA}{dt} \tag{2}$$

Here, the first equation defines the radius, R, of an equivalent circle which has the same area, A, as the spherulite, whereas the second relates the growth velocity, G, directly to the time evolution of area, A. To use the above equations, spherulite images from each experiment were converted into the binary form using the ImageJ software[61] and the areas of the spherulites were measured. The A vs t data were then fitted to a polynomial, and R and G were then obtained from the polynomial using the above equations. Further details related to the data analysis can be found in the Supporting Information (Figure S2).

3. RESULTS AND DISCUSSION

3.1. Bulk Crystallization Kinetics. To understand the effects of temperature on the rate and degree of crystallization, volume changes of mixtures of POCB and water were measured in a custom volume dilatometer as described above. Samples consisting of an 8−23.6% by weight mixture of POCB in water were topped with a layer of mineral oil. In a typical experiment, the preloaded dilatometer was transferred from a bath held at a temperature above the melting point (48 °C) to a bath held at a fixed crystallization temperature T_c, ranging from 8 to 22 °C.

Two stages of volume contraction were observed (Figure 2a). The first occurred over the course of several minutes regardless of crystallization temperature and is associated with thermal contraction as the sample cools from 48 °C to T_c. The second stage of volume contraction is due to crystallization and accelerates with decreasing T_c. The volume change due to crystallization can be isolated from the total by subtracting the thermal contraction according to eq 3

$$\Delta V_c(t) = -(\Delta V_{total}(t) - \Delta V_{tc}(t)) \tag{3}$$

where the subscripts tc and c refer to "thermal contraction" and "crystallization," respectively. The negative sign ensures that $\Delta V_c(t)$ is presented as a positive value. The following two paragraphs describe how $\Delta V_{tc}(t)$ is estimated, using Figure 2a as an illustrative example.

Two methods were used to determine $\Delta V_{tc}(t)$, depending on the degree of temporal separation between the thermal contraction and the crystallization. At relatively high T_c ($T_c \geq$ 16 °C in Figure 2a), $\Delta V_{total}(t)$ shows an unambiguous plateau after roughly 300 s. Further volume change due to crystallization occurs at times much longer than 500 s, indicating that crystallization is far slower than thermal contraction. In such cases, the data for t < 500 s were fitted to a stretched exponential

$$\Delta V_{tc} = A\left(1 - \exp\left(-\left(\frac{t}{\tau}\right)^m\right)\right) \tag{4}$$

Here, the fitting parameters are the magnitude of the thermal contraction, A, the time constant, τ, and the constant, m. The corresponding fits to eq 4 are shown for $T_c \geq$ 16 °C as dashed lines in Figure 2a. Typically, $\tau \approx$ 66 s and $m \approx$ 0.91.

At lower T_c, crystallization is sufficiently fast that eq 4 cannot be reliably fitted to the first 500 s of $\Delta V_{total}(t)$, i.e., there is no clear plateau in $\Delta V_{total}(t)$ before crystallization starts because the two processes occur at similar rates. In such cases, $\Delta V_{tc}(t)$ is determined by estimating parameters in eq 4. From the $T_c \geq$ 16 °C data, we know that parameter A, which is the magnitude of the thermal contraction, varies linearly with temperature (Figure 2b), and hence the values of A below 16 °C can be obtained readily by extrapolation. The parameters τ and m were found to be almost independent of T_c, and hence their average values from experiments at $T_c \geq$ 16 °C were adopted for T_c < 16 °C. These calculated $\Delta V_{tc}(t)$ are shown as dotted lines.

Having obtained $\Delta V_{tc}(t)$, $\Delta V_c(t)$ was calculated from eq 3. $\Delta V_c(t)$ was then normalized by sample mass to give the specific volume change of crystallization, $\Delta v_c(t)$, which is shown in Figure 2c for the mixture with 15% water. The above procedure was applied to all water contents, and examples for mixtures with 18 and 20% water are shown in Figure 2d,e.

At even lower temperatures, the kinetics of crystallization were sufficiently fast that significant crystallization occurred over the same timescale as temperature equilibration. As crystallization at these temperatures is non-isothermal, such data were not collected.

As is typical for isothermal crystallization, the $\Delta v_c(t)$ vs $\log(t)$ plots of Figure 2c−e are sigmoidal wherein the long-time plateau reflects the volume change Δv_c^{final} associated with complete crystallization, and the time required to approach this plateau reflects the kinetics of crystallization. For samples with relatively slow rates, crystallization did not reach completion within the time frame of data collection, and thus no plateau was observed.

We now analyze the dilatometric data quantitatively. We first examine how Δv_c^{final} changes with water content. Next, we examine how the kinetics (as gauged by the time needed to reach a specified Δv_c) depends on composition and temperature. Finally, we visualize the $\Delta v_c(t)$ data in the form of an Avrami plot.

To obtain Δv_c^{final}, the following procedure was adopted. As it was impractical to follow all experiments to full crystallization, the 3 h time point was selected to highlight the differences in crystallization with water content and temperature. Figure S4 shows the value $\Delta v_c(t)$ at t = 3 h as a function of T_c. At all water contents, Δv_c(3 h) increases with decreasing T_c but plateaus at low T_c values. This behavior suggests that at sufficiently low temperatures, each sample had crystallized to its fullest extent within 3 h, i.e., a longer crystallization time would not result in more crystallization. The low-temperature plateau value estimated from Figure S4 is adopted as the Δv_c^{final}

https://doi.org/10.1021/acsapm.1c01626
ACS Appl. Polym. Mater. 2022, 4, 703−713

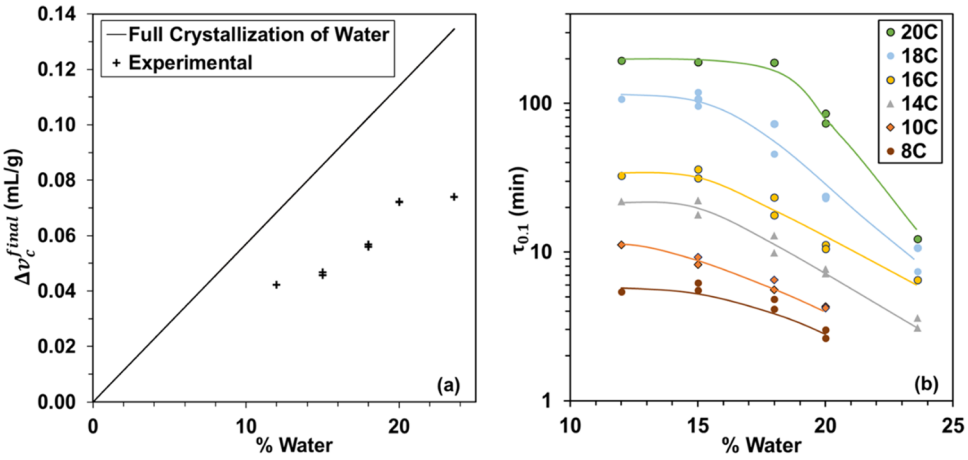

Figure 3. (a) Volume change Δv_c^{final} at various water contents. The solid line corresponds to full crystallization of water, eq 4. (b) Time required for $\Delta v_c = 0.1 v_c^{final}$, i.e., to reach 10% of the final volume change.

and is plotted in Figure 3a. At or below 10% water, Δv_c^{final} values are not reported because these samples did not crystallize fully even at the lowest temperatures and the longest times examined. Not surprisingly, the Δv_c^{final} increases with increasing water content, reflecting the fact that water is the limiting species for hydrate formation.

The experimental Δv_c^{final} was then compared with the theoretical volume change (assuming complete crystallization of all water, Δv_c^{max}), which is given as

$$\Delta v_c^{max} = \left(\frac{m_w}{\rho_w} + \frac{1 - m_w}{\rho_{POCB}}\right) - \left[\frac{m_w/23.6}{\rho_c} + \frac{1 - m_w/23.6}{\rho_{POCB}}\right] \quad (5)$$

where ρ_w, ρ_{POCB}, and ρ_c are the densities of the water, POCB, and crystal, respectively, and 23.6 is the mass percent of water in the crystal. Here, the first bracket is the specific volume of the liquid prior to crystallization (assuming no volume change of mixing), and the latter bracket is the sum of the volumes of the crystal and the uncrystallized POCB. The density of the crystal, estimated from dimensions of the unit cell,[2] is ρ_c = 1.176 g/mL, whereas ρ_{POCB} = 1.02 g/mL and ρ_w = 1.00 g/mL. All three densities are taken as independent of temperature.

A comparison of the data with eq 5 (solid line in Figure 3a) shows that not all water present in the sample crystallizes and some water remains dissolved in the POCB-rich liquid phase even when water is the limiting species (m_w < 23.6%). Note however that this judgment is acutely sensitive to any inaccuracies in ρ_c. In fact, using ρ_c = 1.14 g/mL (rather than 1.176 g/mL) brings the prediction of eq 5 close to the experimental results. Such a 3% error in density would occur with even a 1% deviation of the actual unit cell dimensions from the reported values.

Turning to crystallization kinetics, we define $\tau_{0.1}$ as the time at which $\Delta v_c(t)$ reaches 10% of its final value, i.e., $\Delta v_c(t = \tau_{0.1}) = 0.1\Delta v_c^{final}$. The $\tau_{0.1}$ value provides a simple metric to judge the relative crystallization rates across all samples. Figure 3b shows that $\tau_{0.1}$ increases, i.e., crystallization rate decreases with both increasing temperature and with decreasing water content. At the lowest water contents, however, $\tau_{0.1}$ does not increase any further, i.e., crystallization becomes independent of water content. A similar analysis for $\tau_{0.5}$, i.e., the time needed for half of the final volume change, shows the same trends (Figure S5). This trend indicates that the crystallization mechanism is likely limited by water diffusion at lower water contents.

Finally, moving beyond a single-number metric of $\tau_{0.1}$, we consider the details of how Δv_c evolves with time. The volume changes associated with crystallization can often be described by the Avrami equation[28]

$$\frac{\Delta v_c(t)}{\Delta v_c^{final}} = 1 - \exp(-(kt^n)) \quad (6)$$

where k is the rate coefficient and n is the Avrami exponent. To test whether the Avrami equation can describe hydrate formation in this cocrystallization system, the data were plotted in the linearized form commonly used in the literature

$$\ln\left(-\ln\left(1 - \frac{\Delta v_c(t)}{\Delta v_c^{final}}\right)\right) = n \ln(t) + \ln(k) \quad (7)$$

A plot of the left-hand side of eq 7 vs $\ln(t)$ is expected to give a straight line with a slope equal to the Avrami exponent n. Figure 4 shows an example for the specific case of m_w = 18% (same data as Figure 2d). Similar plots for other compositions are shown in Figure S6. As previously described by others,[28,44] such plots are highly sensitive to small errors in Δv_c early in the crystallization process, e.g., any uncertainties associated with

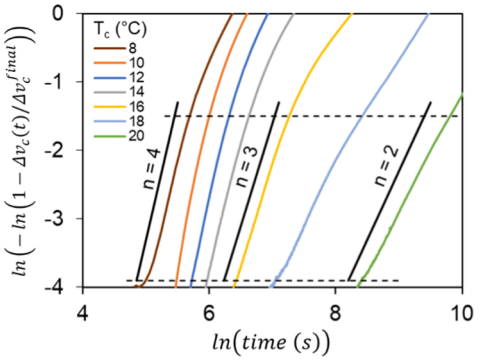

Figure 4. Avrami plots in the form of eq 7 at m_w = 18%. The data are identical to Figure 2d. Lower and upper dashed lines, respectively, correspond to $\Delta v_c/\Delta v_c^{final}$ values of 0.02 and 0.2.

https://doi.org/10.1021/acsapm.1c01626
ACS Appl. Polym. Mater. 2022, 4, 703−713

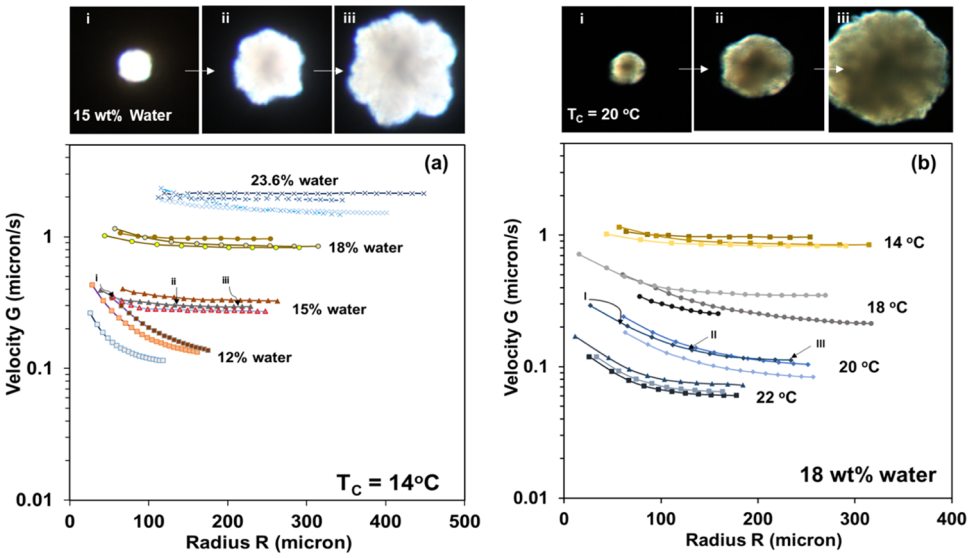

Figure 5. Velocity during spherulite growth in POCB−water mixtures (a) of various compositions at T_c = 14 °C and (b) at various temperatures T_c for a fixed composition m_w = 18% water. Each experiment was conducted three times, and each run is shown separately. Example images at three stages of spherulite growth are shown above.

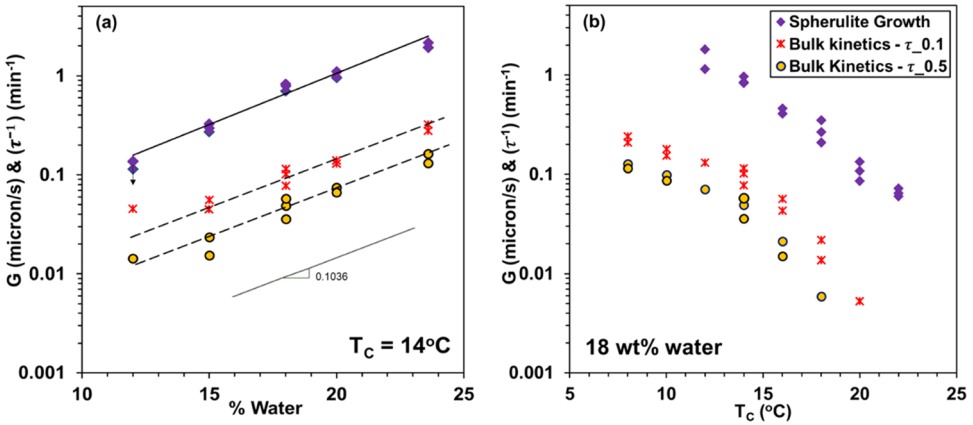

Figure 6. Dependence of steady-state growth velocity (a) on composition m_w (at fixed T_c = 14 °C) and on (b) T_c (at fixed m_w = 18% water). The $\tau_{0.1}$ are the same data as in Figure 3b.

subtracting the thermal contraction in eq 3. Accordingly, data at very early stages $\frac{\Delta v_c(t)}{\Delta v_c^{final}} < 0.02$ are not shown in Figure 4.

The data in Figures 4 and S6 show approximately linear behavior during the early stages of crystallization. At later stages there is a decrease in slope that is consistent both with the behavior seen in homopolymers[28,44] and with the reduction in crystallization rate that is expected due to the depletion of water in bulk as the crystallization proceeds. At all compositions, the early-time slopes are close to $n = 4$ at low T_c, and close to $n = 2$ at high T_c. Further, at fixed T_c, n values generally increase with increasing water content, m_w. The same conclusions are reached if the data are plotted in the Goler-Sachs form[28] ($\ln(\Delta v_c/\Delta v_c^{final})$ vs $\ln(t)$), not shown. Additionally, the n values were insensitive to small changes in the value of Δv_c^{final}. The drift downwards to a lower n value from $n = 4$ to $n = 2$ as T_c increases is consistent with a shift toward a diffusion-controlled mechanism. Moreover, as discussed later, we do not see a shift toward lower dimensionalities of growth by optical microscopy.

A modified Avrami analysis is sometimes adopted[44,62] for polymer crystallization where

$$\frac{\Delta v_c(t)}{\Delta v_c^{final}} = 1 - \exp(-(k(t-t_{ind})^n)) \quad (8)$$

Here, the time t_{ind} is an induction time, i.e., a time delay before the crystallization starts. Induction times typically increase as T_c increases.[62−64] We reanalyzed the data using eq 8 in two variations. In one variation, t_{ind} was selected to be 200 s, which roughly corresponds to the timescale needed for the sample to cool to within 1 °C of the final temperature, T_c. This approach is based on the idea that because crystallization accelerates sharply with reducing temperature, all crystallization will occur only after the sample temperature is close to the target T_c value. This modification reduces the n value for fast-crystallizing samples but has no effect on the n value for slow-crystallizing samples. In the second variation, t_{ind} was set arbitrarily to $\tau_{0.1}/3$, which caused the n value to decrease in all cases. Uncertainties in what value of t_{ind} to use, or indeed whether t_{ind} should simply be set to zero, cause corresponding uncertainties in the absolute values of n. Nevertheless, the overall conclusion—that n reduces as T increases—was found to be valid, independent of the choice of t_{ind}.

https://doi.org/10.1021/acsapm.1c01626
ACS Appl. Polym. Mater. 2022, 4, 703−713

3.2. Spherulite Growth Velocity in the Isothermal Crystallization Process. Even a cursory examination of dilatometers during crystallization showed the presence of spherulites. The growth of these spherulites could be monitored under a polarization microscope in a film geometry. As in all polymer crystallization, one may expect that spherulite growth velocities increase significantly with decreasing temperature T_c. Further, since crystallization requires both water and POCB, one may also expect the growth velocity to depend on mixture composition. This section quantifies the dependence of spherulite growth velocity (G) on T_c at one fixed composition, and on composition at one fixed crystallization temperature.

The evolution of G with spherulite radius is shown in Figure 5a at a single crystallization temperature (T_c = 14 °C) for various compositions and in Figure 5b at a single composition (m_w = 18% water) for various temperatures. Example images of growing spherulites are shown above each graph. In many cases, G initially decreases as the spherulite grows. In most experiments, a steady growth velocity is reached at long times. In some experiments, before a clear steady state is reached, the growing spherulite may impinge upon another spherulite or may grow beyond the field of view. For such samples, the last measured value of G is shown in Figure 5a,b. We will discuss steady velocities first and growth-dependent changes in G next.

Figure 6a shows that the steady growth velocity increases with increasing water content, and the dependence of G on m_w is almost exponential, as shown by the solid line. Figure 6a also plots the bulk crystallization rate, as represented by $\tau_{0.1}^{-1}$ and $\tau_{0.5}^{-1}$, at 14 °C. The slope of the dashed line is the same as of the solid line indicating that over most of the composition range, G, and the bulk crystallization rate have the same composition dependence. Figure 6b shows that G decreases as T_c increases. The qualitative trend is similar to the decrease in $\tau_{0.1}^{-1}$ and $\tau_{0.5}^{-1}$ with temperature (once again, the data in Figure 6a are identical to those in Figure 3b).

The temperature dependence of growth velocity is often well described by the Hoffman–Lauritzen theory that predicts an exponential dependence of G on $T_m/(T_c\Delta T)$, where $\Delta T = (T_m - T_c)$ is the undercooling. Figure 7 plots the velocity data in the form suggested by this theory. Note that since T_m = 310 K and T_c ranges from 283 to 295 K, the term T_m/T_c is nearly constant and close to 1. Accordingly, the x-axis in Figure 7 is nearly identical to $100/\Delta T$. The solid line is a fit to

$$\log_{10} G = A + B\frac{T_m}{T_c\Delta T} \tag{9}$$

where the temperature-coefficient $B = -0.534 \times 10^{-2}$ K^{-1}, which is the slope of the Hoffman–Lauritzen plot, quantifies the sensitivity of the growth velocity to the undercooling. The bulk crystallization rates $\tau_{0.1}^{-1}$ and $\tau_{0.5}^{-1}$ are plotted on the same graph. At high undercooling, the data can be well fitted with a line of the slope of B (dashed line), i.e., the bulk crystallization kinetics have roughly the same temperature dependence as the growth velocity. At low undercooling, however, $\tau_{0.1}^{-1}$ and $\tau_{0.5}^{-1}$ decrease more steeply as ΔT reduces. These results may be approximated by two straight lines (not shown), suggesting a regime change[65−68] with increasing undercooling.

The increase in the temperature dependence of the $\tau_{0.1}^{-1}$ vs $\frac{T_m}{T_c\Delta T}$ data at low undercooling appears at all compositions (Figure S7). At sufficiently large undercoolings, the data for all compositions can be approximated with the same slope of B. With increasing T_c, there is a transition to a higher slope, and the transition seems to occur at lower temperatures at lower water content. We speculate that this behavior may be attributable to a sharp decrease in primary nucleation rate as T_c approaches the melting temperature T_m or as water content reduces. Notably, such a decrease in primary nucleation rate would not affect the slope of the G vs $\frac{T_m}{T_c\Delta T}$ data, which is consistent with Figure 7. Alternatively, this transition may otherwise represent a steady-state growth velocity dependency change from diffusion-limited growth to reaction-limited growth. We also note that G vs $\frac{T_m}{T_c\Delta T}$ cannot be plotted at as low of undercoolings as $\tau_{0.1}^{-1}$ vs $\frac{T_m}{T_c\Delta T}$ due to the logistics of locating a newly formed spherulite under a microscope, thus while there appears to be no transition for the microscopic data, it may just not be present at temperatures plotted.

Finally, we turn to the observation from Figure 5 that in many cases, G decreases at a decreasing rate during spherulite growth. In homopolymer systems under isothermal conditions,[29,69] spherulites grow at a constant radial growth velocity. However, in multicomponent systems, the presence of impurities in the melt can reduce G as spherulites grow.[31] The impurities must be excluded from the crystals and, if growth is sufficiently slow, the impurities may be rejected from the spherulite altogether. This exclusion leads to the gradual buildup of a high concentration of impurity at the spherulite growth front, hence reducing G. Eventually, a steady state may be reached such that the spherulitic growth rate matches the rate at which the impurity diffuses away from the interface. The POCB–water cocrystal has 23.6 wt % water,[1] corresponding to 1:1 molar ratio of monomer repeat unit to water, and therefore in all samples with m_w < 23.6% water, the excess POCB must be rejected. Excess POCB can then be viewed to have the same effect as an impurity. Moreover, lower values of m_w require larger quantities of POCB to be rejected. Rejection of the POCB would cause a decrease in G until an eventual diffusion-limited steady-state growth is reached. The experiments agree with these expectations. Specifically, Figure 5 shows that the decrease in G is much larger at low water contents, i.e., at compositions in which a larger quantity of POCB must be rejected from the crystallization mixture.

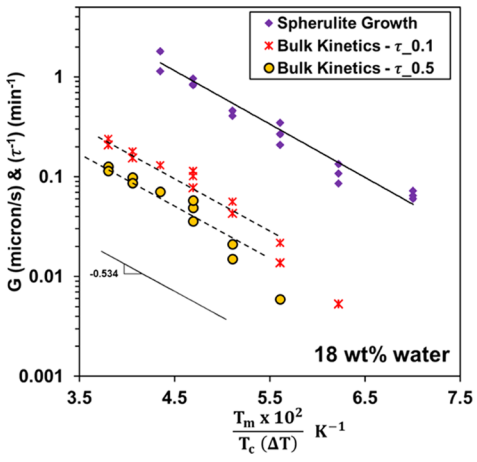

Figure 7. Spherulite growth velocity and bulk kinetics of mixtures with m_w = 18% water in the form of a Hoffman–Lauritzen plot.

https://doi.org/10.1021/acsapm.1c01626
ACS Appl. Polym. Mater. 2022, 4, 703−713

Although most samples reach a steady growth velocity in our experiments, the behavior of G at long times depends strongly on composition. For the sample with 23.6% water, spherulites stop growing when they impinge on each other. However, for nonstoichiometric mixtures, we expect growth would eventually slow down because the available water is exhausted even before impingement. Such nonimpinging spherulites are well-documented in the literature on crystallization of homopolymers with impurities.[29] In such cases, G must eventually reduce to zero prior to impingement. However, this corresponds to very large spherulites that are too large to be captured within the field of view of the microscope, and thus a decrease in G toward zero is not seen in Figure 5.

For all compositions and temperatures, spherulites were observed and axialites were not seen (Figure S8). That is, no change in growth mechanism was apparent from qualitative microscopic observation. At late stages during crystallization (beyond the times considered in the analysis here), the spherulites sometimes showed flowerlike shapes, which have also been seen previously.[30,37,70] Because the above analysis solely focused on the early stage spherulites, this type of shape did not affect the quantitative results presented above.

3.3. Effect of Nucleating Agent. Particulate nucleating agents are often used to accelerate crystallization kinetics. Accordingly, we tested two candidates as nucleating agents, hydrophilic fumed silica and talc. Experiments were conducted in mixtures with m_w = 18% at three different temperatures. Figure 8a shows that the crystallization kinetics of samples with fumed silica is similar to those without particles. The same figure shows that at 19 and 21 °C, there is a several-fold acceleration in the bulk kinetics for the sample with talc. At 15 °C, the sample with talc crystallized so rapidly that the first plateau corresponding to ΔV_{tc} was not visible at all. This lack of a visible plateau due to thermal contraction indicates that the crystallization was not isothermal, i.e., significant crystallization occurred even before the sample reached 15 °C. As such, those data are not shown in Figure 8a. The photos in Figure 8b–d show the samples at the end of the crystallization process. While mm-scale spherulites are visible in the sample without particles or with fumed silica, the sample with talc shows a smooth milky appearance, suggesting small spherulites, consistent with the idea that talc accelerates primary nucleation.

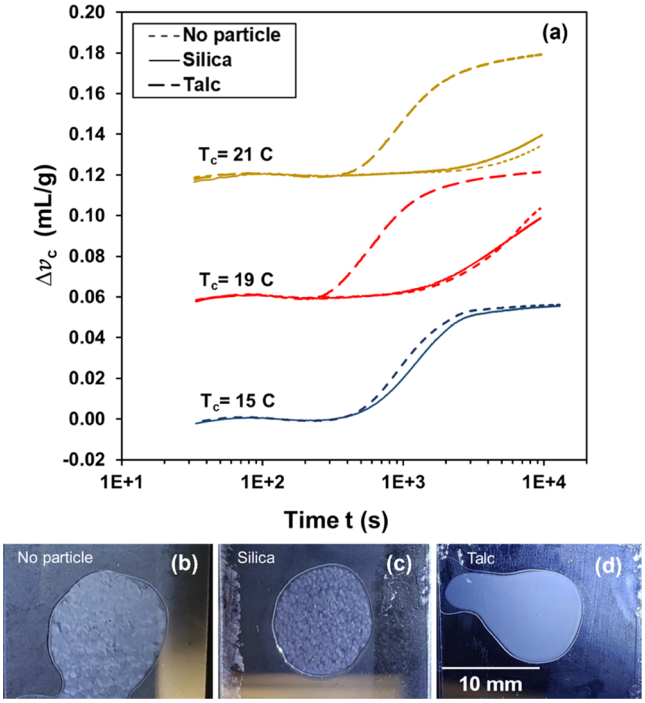

Figure 8. (a) Effect of nucleating agent on crystallization kinetics of samples with m_w = 18% at three different temperatures. For clarity, each set of curves is shifted upwards with respect to the previous set by 0.06 mL/g. (b–d) Images of three samples with and without particles after crystallization at T_c = 15 °C for 30 min.

4. SUMMARY AND CONCLUSIONS

In summary, polyoxacyclobutane has the rare ability to cocrystallize with water to form a hydrate. We report the first study of the kinetics of POCB hydrate cocrystallization, and indeed the first study of cocrystallization kinetics of any polymer with a small molecule. This paper is restricted to water contents below 24 wt % at which POCB–water mixtures form single-phase homogeneous liquid prior to crystallization. We examine the kinetics of bulk hydrate crystallization by dilatometry and the kinetics of spherulite growth by polarization microscopy. The central issues of interest are the dependence of cocrystallization kinetics on temperature and on mixture composition.

The central conclusions of the paper are:

(1) The time evolution of the bulk kinetics can be described by the Avrami equation, with the Avrami exponent reducing from roughly 4 to 2 as undercooling reduces.

(2) The bulk crystallization rate, as quantified by the reciprocal of time needed to reach 10% crystallization, decreases exponentially as the water content reduces and decreases exponentially as ΔT^{-1} increases, where ΔT is the undercooling.

(3) At dilute water content, spherulite growth velocity reduces from a high initial value to a steady-state value, reminiscent of homopolymer crystallization with impurities. This analysis suggests that the excess POCB (as the nonlimiting species) acts as an impurity, causing diffusion barriers to hydrate crystallization.

(4) The dependence of bulk crystallization rate on composition and temperature mirrors that of steady-state spherulite growth velocity at high undercooling. However, at low undercooling, the bulk rate shows a sharper temperature dependence, whereas spherulite growth velocity does not. We speculate that this apparent regime change in the bulk kinetics, but not in the spherulite growth velocity, may be due to either a sharp decrease in primary nucleation kinetics or due to standard explanations of regime changes (secondary nucleation occurring at a similar order of magnitude as lateral growth) that are not represented in the growth velocity data due to the difficulty in collecting low-temperature spherulite images.

(5) Talc is an effective nucleating agent for POCB hydrate crystallization, but fumed silica is not.

Overall, we conclude that the mechanism of cocrystallization is three-dimensional (3D) spherulitic growth wherein the rate of primary nucleation and spherulite growth velocity both reduce with increasing temperature or decreasing water content. The growth velocity slows down as the spherulite grows due to diffusion limitations as one of the two

https://doi.org/10.1021/acsapm.1c01626
ACS Appl. Polym. Mater. 2022, 4, 703–713

cocrystallizing species becomes depleted. We were able to apply well-established kinetic models in the homopolymer literature to cocrystallization to analyze the mechanism. The bulk crystallization kinetics data can be well fitted by the JMAK model, and the temperature dependence of spherulite growth velocity is consistent with the Hoffman–Lauritzen model. At least one other polymer is known to cocrystallize with water, and many more cocrystallize with other small molecules, although cocrystallization kinetics have not been reported. This paper suggests that when the mixture is a homogeneous liquid prior to cocrystallization, the process resembles homopolymer crystallization. Yet, the dependence of kinetics on composition is a necessary complexity in such systems, i.e., as the mixture composition deviates from the cocrystal stoichiometry, the excess species must act as an impurity causing diffusion limitations. Our ongoing work focuses on hydrate crystallization kinetics at high water contents at which POCB–water mixtures are in liquid–liquid equilibrium prior to crystallization. We anticipate that, in that case, the crystallization process will be heavily influenced by mixing conditions.

■ ASSOCIATED CONTENT

Supporting Information

The Supporting Information is available free of charge at https://pubs.acs.org/doi/10.1021/acsapm.1c01626.

Experimental procedures, data, data analysis, and apparatus images (PDF)

■ AUTHOR INFORMATION

Corresponding Authors

Tara Y. Meyer − *Department of Chemistry, University of Pittsburgh, Pittsburgh, Pennsylvania 15260, United States;* orcid.org/0000-0002-9810-454X; Email: tmeyer@pitt.edu

Sachin Velankar − *Department of Chemical Engineering, Department of Mechanical Engineering and Materials Science, University of Pittsburgh, Pittsburgh, Pennsylvania 15250, United States;* orcid.org/0000-0001-7541-1355; Email: velankar@pitt.edu

Authors

Emily F. Barker − *Department of Chemistry, University of Pittsburgh, Pittsburgh, Pennsylvania 15260, United States;* orcid.org/0000-0003-1674-0313

Sudesna Banerjee − *Department of Chemical Engineering, Department of Mechanical Engineering and Materials Science, University of Pittsburgh, Pittsburgh, Pennsylvania 15250, United States;* orcid.org/0000-0002-9535-405X

Complete contact information is available at: https://pubs.acs.org/10.1021/acsapm.1c01626

Author Contributions

[§]E.F.B. and S.B. contributed equally. The manuscript was written through the contributions of all authors. All authors have given approval to the final version of the manuscript.

Funding

This research was supported by the National Science Foundation Award (CBET 1933037).

Notes

The authors declare no competing financial interest.

■ ACKNOWLEDGMENTS

The authors thank Dr. Hari Sunkara from Dupont for making the POCB available, Dylan Butler for assisting with the design of the dilatometer holder, and R. Venkat Raman, Sastra University, for assisting with the design of the dilatometer holder and carrying out preliminary experiments.

■ REFERENCES

(1) Banerjee, J.; Koronaios, P.; Morganstein, B.; Geib, S. J.; Enick, R. M.; Keith, J. A.; Beckman, E. J.; Velankar, S. S. Liquids That Freeze When Mixed: Cocrystallization and Liquid–Liquid Equilibrium in Polyoxacyclobutane–Water Mixtures. *Macromolecules* **2018**, *51*, 3176–3183.

(2) Kakida, H.; Makino, D.; Chatani, Y.; Kobayashi, M.; Tadokoro, H. Strutural studies of polyethers [-(CH2) mO-] n. viii. polyoxacyclobutane hydrate (modification i). *Macromolecules* **1970**, *3*, 569–578.

(3) Yoshida, S.; Sakiyama, M.; Seki, S. Thermodynamic Studies of Solid Polyethers. I. Poly (oxacyclobutane),[−(CH 2) 3 O−] n and Its Hydrate. *Polym. J.* **1970**, *1*, 573–581.

(4) Takahashi, Y.; Osaki, Y.; Tadokoro, H. Planar zigzag modification of polyoxacyclobutane (modification IV) and its disordered structure1. *J. Polym. Sci., Part B: Polym. Phys.* **1981**, *19*, 1153–1155.

(5) Tadokoro, H.; Takahashi, Y.; Chatani, Y.; Kakida, H. Structural studies of polyethers, [-(CH2)m-O-]n. V. Polyoxacyclobutane. *Makromol. Chem.* **1967**, *109*, 96–111.

(6) Tarallo, O. *Encyclopedia of Polymer Science and Technology*; Wiley Online Library, 2002.

(7) Guenet, J.-M. *Polymer-Solvent Molecular Compounds*; Elsevier, 2010.

(8) Malik, S.; Rochas, C.; Schmutz, M.; Guenet, J. M. Syndiotactic Polystyrene Intercalates from Naphthalene Derivatives. *Macromolecules* **2005**, *38*, 6024–6030.

(9) Dasgupta, D.; Malik, S.; Thierry, A.; Guenet, J. M.; Nandi, A. K. Thermodynamics, Morphology, and Structure of the Poly(vinylidene fluoride)–Ethyl Acetoacetate System. *Macromolecules* **2006**, *39*, 6110–6114.

(10) Tarallo, O.; Petraccone, V.; Albunia, A. R.; Daniel, C.; Guerra, G. Monoclinic and Triclinic δ-Clathrates of Syndiotactic Polystyrene. *Macromolecules* **2010**, *43*, 8549–8558.

(11) Point, J.; Coutelier, C. Linear high polymers as host in intercalates. Introduction and example. *J. Polym. Sci., Part B: Polym. Phys.* **1985**, *23*, 231–239.

(12) Paternostre, L.; Damman, P.; Dosière, M. Metastabilities of lamellar crystals of molecular complexes. *Polymer* **1998**, *39*, 4579–4592.

(13) Delaite, E.; Point, J. J.; Damman, P.; Dosiere, M. Two allotropic forms for the poly(ethylene oxide)-resorcinol molecular complex. *Macromolecules* **1992**, *25*, 4768–4778.

(14) Wagner, J. F.; Dosière, M.; Guenet, J. M. *Temperature-Concentration Phase Diagram of PEO-Urea*; Macromolecular Symposia, Wiley Online Library, 2005; pp 121–124.

(15) Belfiore, L. A.; Lee, C. K.; Tang, J. The influence of competitive interactions on multiple eutectic phase behavior in poly (ethylene oxide) molecular complexes. *Polymer* **2003**, *44*, 3333–3346.

(16) Sasaki, S.; Takahashi, Y.; Tadokoro, H. Structural studies of polyformals. II. Crystal structure of poly-1,3-dioxolane: Modification II1. *J. Polym. Sci., Part B: Polym. Phys.* **1972**, *10*, 2363–2378.

(17) Alamo, R.; Fatou, J. G.; Guzmán, J. Crystallization of polyformals: 1. Crystallization kinetics of poly(1,3-dioxolane). *Polymer* **1982**, *23*, 374–378.

(18) Benkhira, A.; Franta, E.; Francois, J. Polydioxolane in aqueous solutions. 1. Phase diagram. *Macromolecules* **1992**, *25*, 5697–5704.

(19) Chatani, Y.; Kobatake, T.; Tadokoro, H. Structural studies of poly (ethylenimine). 3. Structural characterization of anhydrous and hydrous states and crystal structure of the hemihydrate. *Macromolecules* **1983**, *16*, 199–204.

(20) Chido, M. T.; Koronaios, P.; Saravanan, K.; Adams, A. P.; Geib, S. J.; Zhu, Q.; Sunkara, H. B.; Velankar, S. S.; Enick, R. M.; Keith, J. A.; Star, A. Oligomer hydrate crystallization improves carbon nanotube memory. *Chem. Mater.* **2018**, *30*, 3813−3818.
(21) Badeau, B. A.; DeForest, C. A. Programming Stimuli-Responsive Behavior into Biomaterials. *Annu. Rev. Biomed. Eng.* **2019**, *21*, 241−265.
(22) Municoy, S.; Álvarez Echazú, M. I.; Antezana, P. E.; Galdopórpora, J. M.; Olivetti, C.; Mebert, A. M.; Foglia, M. L.; Tuttolomondo, M. V.; Alvarez, G. S.; Hardy, J. G.; Desimone, M. F. Stimuli-Responsive Materials for Tissue Engineering and Drug Delivery. *Int. J. Mol. Sci.* **2020**, *21*, 4724.
(23) Babu, P.; Nambiar, A.; He, T.; Karimi, I. A.; Lee, J. D.; Englezos, P.; Linga, P. A review of clathrate hydrate based desalination to strengthen energy−water nexus. *ACS Sustainable Chem. Eng.* **2018**, *6*, 8093−8107.
(24) Gadjourova, Z.; Andreev, Y. G.; Tunstall, D. P.; Bruce, P. G. Ionic conductivity in crystalline polymer electrolytes. *Nature* **2001**, *412*, 520−523.
(25) Freier, E.; Wolf, S.; Gerwert, K. Proton transfer via a transient linear water-molecule chain in a membrane protein. *Proc. Natl. Acad. Sci. U.S.A.* **2011**, *108*, 11435−11439.
(26) Wei, M.; Gao, Y.; Li, X.; Serpe, M. J. Stimuli-responsive polymers and their applications. *Polym. Chem.* **2017**, *8*, 127−143.
(27) Xie, L.; Li, X.-j.; Xiong, Y.-z.; Chen, Q.; Xie, H.-b.; Zheng, Q. Can classic Avrami theory describe the isothermal crystallization kinetics for stereocomplex poly (lactic acid)? *Chin. J. Polym. Sci.* **2017**, *35*, 773−781.
(28) Mandelkern, L. *Crystallization of Polymers: Kinetics and Mechanisms*; Cambridge University Press, 2004; Vol. *2*.
(29) Crist, B.; Schultz, J. M. Polymer spherulites: A critical review. *Prog. Polym. Sci.* **2016**, *56*, 1−63.
(30) Wunderlich, B. *Macromolecular Physics V2*; Elsevier, 2012; Vol. *2*.
(31) Mandelkern, L. Crystallization Kinetics of Polymer Mixtures. In *Crystallization of Polymers: Kinetics and Mechanisms*; Cambridge University Press, 2004; Vol. *2*.
(32) Cao, M.; Xu, J. T.; Dong, Q.; Fu, Z. S.; Fan, Z. Q. Crystallization kinetics and morphology of iso-PP/ethylene-propylene-b-copolymer/ethylene-propylene-r-copolymer ternary blends. *Iran. Polym. J.* **2009**, *18*, 373−382.
(33) Hwang, J. C.; Chen, C.-C.; Chen, H.-L.; Yang, W.-C. O. Analysis of two-stage crystallization kinetics for poly (ethylene terephthalate)/poly (ether imide) blends. *Polymer* **1997**, *38*, 4097−4101.
(34) Huang, J.-W.; Chang, C.-C.; Kang, C.-C.; Yeh, M.-Y. Crystallization kinetics and nucleation parameters of Nylon 6 and poly (ethylene-co-glycidyl methacrylate) blend. *Thermochim. Acta* **2008**, *468*, 66−74.
(35) Zhang, M. C.; Guo, B.-H.; Xu, J. A review on polymer crystallization theories. *Crystals* **2017**, *7*, 4.
(36) Piorkowska, E.; Galeski, A.; Haudin, J.-M. Critical assessment of overall crystallization kinetics theories and predictions. *Prog. Polym. Sci.* **2006**, *31*, 549−575.
(37) Bruna, P.; Crespo, D.; González-Cinca, R.; Pineda, E. On the validity of Avrami formalism in primary crystallization. *J. Appl. Phys.* **2006**, *100*, No. 054907.
(38) Zhang, S.; Han, J.; Gao, Y.; Guo, B.; Reiter, Gn.; Xu, J. Determination of the critical size of secondary nuclei on the lateral growth front of lamellar polymer crystals. *Macromolecules* **2019**, *52*, 7439−7447.
(39) Kundagrami, A.; Muthukumar, M. Continuum theory of polymer crystallization. *J. Chem. Phys.* **2007**, *126*, No. 144901.
(40) Sanchez, I. C.; DiMarzio, E. A. Dilute solution theory of polymer crystal growth: a kinetic theory of chain folding. *J. Chem. Phys.* **1971**, *55*, 893−908.
(41) Sadler, D. M. New explanation for chain folding in polymers. *Nature* **1987**, *326*, 174−177.
(42) Sadler, D. M.; Gilmer, G. H. Selection of lamellar thickness in polymer crystal growth: a rate-theory model. *Phys. Rev. B* **1988**, *38*, 5684.
(43) Evans, U. The laws of expanding circles and spheres in relation to the lateral growth of surface films and the grain-size of metals. *Trans. Faraday Soc.* **1945**, *41*, 365−374.
(44) Lorenzo, A. T.; Arnal, M. L.; Albuerne, J.; Müller, A. J. DSC isothermal polymer crystallization kinetics measurements and the use of the Avrami equation to fit the data: Guidelines to avoid common problems. *Polym. Test.* **2007**, *26*, 222−231.
(45) Pradell, T.; Crespo, D.; Clavaguera, N.; Clavaguera-Mora, M. Diffusion controlled grain growth in primary crystallization: Avrami exponents revisited. *J. Phys.: Condens. Matter* **1998**, *10*, 3833.
(46) Mandelkern, L. Crystallization Kinetics of Homopolymers: Bulk Crystallization; Mathematical Formulation. In *Crystallization of Polymers: Kinetics and Mechanisms*; Cambridge University Press, 2004; Vol. *2*.
(47) Rodrigues, M.; Baptista, B.; Lopes, J. A.; Sarraguça, M. C. Pharmaceutical cocrystallization techniques. Advances and challenges. *Int. J. Pharm.* **2018**, *547*, 404−420.
(48) Nugrahani, I.; Utami, D.; Ibrahim, S.; Nugraha, Y. P.; Uekusa, H. Zwitterionic cocrystal of diclofenac and l-proline: structure determination, solubility, kinetics of cocrystallization, and stability study. *Eur. J. Pharm. Sci.* **2018**, *117*, 168−176.
(49) Padrela, L.; Rodrigues, M. A.; Tiago, Jo.; Velaga, S. P.; Matos, H. A.; de Azevedo, E. G. Insight into the mechanisms of cocrystallization of pharmaceuticals in supercritical solvents. *Cryst. Growth Des.* **2015**, *15*, 3175−3181.
(50) Sarcevič a, I.; Orola, Ln.; Nartowski, K. P.; Khimyak, Y. Z.; Round, A. N.; Fábián, L. Mechanistic and Kinetic Insight into Spontaneous Cocrystallization of Isoniazid and Benzoic Acid. *Mol. Pharmaceutics* **2015**, *12*, 2981−2992.
(51) Xanthopoulou, M.; Giliopoulos, D.; Tzollas, N.; Triantafyllidis, K. S.; Kostoglou, M.; Katsoyiannis, I. A. Phosphate removal using polyethylenimine functionalized silica-based materials. *Sustainability* **2021**, *13*, 1502.
(52) Thakur, A. K.; Nisola, G. M.; Limjuco, L. A.; Parohinog, K. J.; Torrejos, R. E. C.; Shahi, V. K.; Chung, W.-J. Polyethylenimine-modified mesoporous silica adsorbent for simultaneous removal of Cd(II) and Ni(II) from aqueous solution. *J. Ind. Eng. Chem.* **2017**, *49*, 133−144.
(53) Tang, Y.; Li, M.; Mu, C.; Zhou, J.; Shi, B. Ultrafast and efficient removal of anionic dyes from wastewater by polyethyleneimine-modified silica nanoparticles. *Chemosphere* **2019**, *229*, 570−579.
(54) Bhatnagar, V. Clathrates of urea and thiourea. *J. Struct. Chem.* **1968**, *8*, 513−529.
(55) Harada, A.; Li, J.; Kamachi, M. Double-stranded inclusion complexes of cyclodextrin threaded on poly (ethylene glycol). *Nature* **1994**, *370*, 126−128.
(56) Manfredi, C.; Del Nobile, M.; Mensitieri, G.; Guerra, G.; Rapacciuolo, M. Vapor sorption in emptied clathrate samples of syndiotactic polystyrene. *J. Polym. Sci., Part B: Polym. Phys.* **1997**, *35*, 133−140.
(57) Balijepalli, S.; Schultz, J.; Lin, J. Phase behavior and morphology of poly (ethylene oxide) blends. *Macromolecules* **1996**, *29*, 6601−6611.
(58) Jiang, X.; Li, T.; Hu, W. Understanding the Growth Rates of Polymer Cocrystallization in the Binary Mixtures of Different Chain Lengths: Revisited. *J. Phys. Chem. B* **2015**, *119*, 9975−9981.
(59) Pal, S.; Nandi, A. K. Cocrystallization mechanism of poly (3-hexyl thiophenes) with different amount of chain regioregularity. *J. Appl. Polym. Sci.* **2006**, *101*, 3811−3820.
(60) Datta, J.; Nandi, A. K. Cocrystallization mechanism of vinylidene fluoride-tetrafluoroethylene copolymers with different copolymer composition. *Macromol. Chem. Phys.* **1998**, *199*, 2583−2588.
(61) Schneider, C. A.; Rasband, W. S.; Eliceiri, K. W. NIH Image to ImageJ: 25 years of image analysis. *Nat. Methods* **2012**, *9*, 671−675.

https://doi.org/10.1021/acsapm.1c01626
ACS Appl. Polym. Mater. 2022, 4, 703−713

(62) Iwamatsu, M. Direct numerical simulation of homogeneous nucleation and growth in a phase-field model using cell dynamics method. *J. Chem. Phys.* **2008**, *128*, No. 084504.
(63) Deshpande, V.; Jape, S. Isothermal crystallization kinetics of anhydrous sodium acetate nucleated poly (ethylene terephthalate). *J. Appl. Polym. Sci.* **2010**, *116*, 3541−3554.
(64) Inoue, M. Crystallization and melting of copolymers of polyoxymethylene. *J. Appl. Polym. Sci.* **1964**, *8*, 2225−2238.
(65) Hoffman, J. D.; Frolen, L. J.; Ross, G. S.; Lauritzen, J. I., Jr On the growth rate of spherulites and axialites from the melt in polyethylene fractions: regime I and regime II crystallization. *J. Res. Natl. Bur. Stand., Sect. A* **1975**, *79A*, 671.
(66) Lauritzen, J. I., Jr; Hoffman, J. D. Extension of theory of growth of chain-folded polymer crystals to large undercoolings. *J. Appl. Phys.* **1973**, *44*, 4340−4352.
(67) Rice, S. A. *Advances in Chemical Physics*; Wiley [etc.]: New York, 2004; Vol. *128*.
(68) Allen, R. C.; Mandelkern, L. On regimes I and II during polymer crystallization. *Polym. Bull.* **1987**, *17*, 473−480.
(69) Keith, H. D.; Padden, F. J. A Phenomenological Theory of Spherulitic Crystallization. *J. Appl. Phys.* **1963**, *34*, 2409−2421.
(70) Couder, Y.; Maurer, J.; González-Cinca, R.; Hernández-Machado, A. Side-branch growth in two-dimensional dendrites. I. Experiments. *Phys. Rev. E* **2005**, *71*, No. 031602.

https://doi.org/10.1021/acsapm.1c01626
ACS Appl. Polym. Mater. 2022, 4, 703−713